IFAC

International Federation of Automatic Control

ADVANCES IN AUTOMOTIVE CONTROL 2001

A Proceedings volume from the 3rd IFAC Workshop
Karlsruhe, Germany, 28 - 30 March 2001

Edited by

U. KIENCKE and G.L. GISSINGER

PERGAMON

ADVANCES IN AUTOMOTIVE CONTROL 2001

A Proceedings volume from the 3rd IFAC Workshop, Karlsruhe, Germany, 28 - 30 March 2001

Edited by

U. KIENCKE
University of Karlsruhe, Germany

and

G.L. GISSINGER
University of Haute Alsace, France

Published for the

INTERNATIONAL FEDERATION OF AUTOMATIC CONTROL

by

PERGAMON
An Imprint of Elsevier Science

UK Elsevier Science Ltd, The Boulevard, Langford Lane, Kidlington, Oxford, OX5 1GB, UK
USA Elsevier Science Inc., 660 White Plains Road, Tarrytown, New York 10591-5153, USA
JAPAN Elsevier Science Japan, Tsunashima Building Annex, 3-20-12 Yushima, Bunkyo-ku, Tokyo 113, Japan

Copyright © 2001 IFAC

All Rights Reserved. No part of this publication may be reproduced, stored in a retrieval system or transmitted in any form or by any means: electronic, electrostatic, magnetic tape, mechanical, photocopying, recording or otherwise, without permission in writing from the copyright holders.

First edition 2001

Library of Congress Cataloging in Publication Data

A catalogue record for this book is available from the Library of Congress

British Library Cataloguing in Publication Data

A catalogue record for this book is available from the British Library

ISBN 0-08-043678 1

These proceedings were reproduced from manuscripts supplied by the authors, therefore the reproduction is not completely uniform but neither the format nor the language have been changed in the interests of rapid publication. Whilst every effort is made by the publishers to see that no inaccurate or misleading data, opinion or statement appears in this publication, they wish to make it clear that the data and opinions appearing in the articles herein are the sole responsibility of the contributor concerned. Accordingly, the publisher, editors and their respective employers, officers and agents accept no responsibility or liability whatsoever for the consequences of any such inaccurate or misleading data, opinion or statement.

Printed in Great Britain

3rd IFAC WORKSHOP ON ADVANCES IN AUTOMOTIVE CONTROL 2001

Sponsored by
International Federation of Automatic Control (IFAC)
IFAC Technical Committee on Automotive Control

Co-sponsored by
IFAC Technical Committee on Components and Instruments
VDI/VDE-Gesellschaft Mess- und Verkehrstechnik (FVT)

Organized by
VDI/VDE-Gesellschaft Mess- und Automatisierungstechnik (GMA)
Institute of Industrial Information Technology (IIIT), University of Karlsruhe

International Programme Committee (IPC)

Gissinger, G.(F) (Chairman)

Basset, M. (F)	Boverie, S. (F)
Guzzella, L. (CH)	Hedrick, K. (USA)
Hrovat, D. (USA)	Isermann, R. (D)
Kiencke, U. (D)	Nielsen, L. (S)
Rizzo, G. (I)	Rizzoni, G. (USA)

National Organizing Committee (NOC)

Kiencke, U. (Chairman)
Mueller, H.
Krebs, V.
Ringelmann, A.

Preface

The Third IFAC Workshop ADVANCES IN AUTOMOTIVE CONTROL took place in Karlsruhe, Germany during 28-30 March 2001. This Workshop follows the first two very successful meetings: the 1995 meeting held in Ancona, Switzerland and the 1998 meeting held in the Mohican State Park, Ohio, USA.

As the subject indicates, the aim of this workshop was to discuss not only the latest advances related to motor vehicles, but also, and more generally, to exchange ideas between academic partners, car-manufacturers and subcontractors. No doubt plenary lectures are of great importance and the thematic sessions in the different sectors are the essence of such workshops. However, the discussions between experts in the different fields, the meetings between people from industry, universities and public or private laboratories, as well as the resulting exchange of ideas, are as important.

Research is often criticized for providing merely theoretical results and for the insufficient number of its applications. The motor vehicle offers a wide field of applications in which we can validate all techniques, tools and methods. This allows us to be involved in all the areas of fundamental research, in all the different possible approaches from fundamental research to technology transfer, and to observe the actual effects of our results.

The increase in road traffic was a major problem of the past XXth century. It is clear that one of the challenges of the XXIst century will be to improve driving safety and comfort. The sessions in the Proceedings volume are divided as follows:

- Driveline control
- Driveline modelling
- Vehicle dynamics (I and II)
- Electronic architecture
- Intelligent components
- Engine control (I and II)
- Diagnostics
- Subsystems
- Engine modelling
- Modelling of combustion and turbo-charging

The quality of the papers and the diversity of their origins clearly show the interest that we all take in this key sector of our research and industry.

We wish to thank all the authors for their papers. We also wish to thank our colleagues from IPC for organizing the different sessions and crossed reviews, which are proof of quality within our community. We are particularly grateful to Professor Kiencke's team of the National Organizing Committee, and Mrs Koffler in particular, for their excellent preparatory arrangements and for the practical organization of this workshop. We gratefully acknowledge VDI/VDE-GMA and Mrs Ringelmann in particular for their support without which this workshop could not have been held.

We also recognize the support, financial and otherwise, of IFAC, the University of Karlsruhe and Dspace in making this Workshop possible and so successful.

Gérard L. Gissinger
Uwe Kiencke

此为试读,需要完整PDF请访问: www.ertongbook.com

CONTENTS

DRIVELINE CONTROL

Diesel-Engine Speed Control with Handling of Driveline Resonances 1
M. PETTERSSON, L. NIELSEN

H-Infinity Control and μ-Analysis for Active Control of Vehicle Longitudinal Oscillations 11
D. LEFEBVRE, P. CHEVREL, C. PERRIER

Fuel-Optimal Control of CVT Powertrains 17
R. PFIFFNER, L. GUZZELLA, C.H. ONDER

Optimal Piecewise-Linear Control of Dry Clutch Engagement 23
A. BEMPORAD, F. BORRELLI, L. GLIELMO, F. VASCA

Approximate I/O Linearization of a Continuously Variable Transmission 29
S. HOHMANN, A. SCHÖNBOHM, V. KREBS

VEHICLE DYNAMICS I

Fuzzy Lane-Track Control for the Automatic Guidance of an Automotive Vehicle 35
F. BONNAY, S. BRIAUD, F. COFFIN, Z. ZALILA

Longitudinal Tire Force Estimation Based on Sliding Mode Observer 41
A. EL HADRI, G. BEURIER, J.C. CADIOU, N.K. M'SIRDI, Y. DELANNE

Visual Behaviour Analysis and Driver Cognitive Model 47
J. BAUJON, M. BASSET, G.L. GISSINGER

Effect of the Crone Suspension Control System on Braking 53
X. MOREAU, C. NOUILLANT, A. OUSTALOUP

Human-Friendly Control Design for Drive-By-Wire Steering Vehicles 59
C. CANUDAS-DE-WIT, P. BILLOT

DRIVELINE MODELLING

Simulation of a Vehicle in Longitudinal Motion with Clutch Lock and Clutch Release 65
L. ERIKSSON

The Hardware Are-In-The-Loop Simulation Test of a Parallel Hybrid Transmission Control System 71
J. MARCO, R. BALL, R.P. JONES, A. ROXBURGH

Modeling and Control of Continuously Variable Transmissions 79
C. MÜLLER, D. SCHRÖDER

Modeling and Control of a V-Belt CVT 85
F. ASSADIAN, D. MARGOLIS

Modeling and Analysis of Longitudinal Tire Dynamics Based on the Lugre Friction Model 91
J. DEUR

VEHICLE DYNAMICS II

Robust Vehicle Steering Control Design Based on the Disturbance Observer 97
T. BÜNTE, D. ODENTHAL, B. AKSUN-GÜVENÇ, L. GÜVENÇ

Comparison of Skyhook and H_∞ Control Applied on a Quarter-Car Suspension Model 107
D. SAMMIER, O. SENAME, L. DUGARD

Influences of Braking System Faults on the Vehicle Dynamics 113
H. STRAKY, M. KOCHEM, J. SCHMITT, R. HILD, R. ISERMANN

Modeling of Vehicles Using Robotics Formulation 119
É. GUILLO, M. GAUTIER

Feedforward and Feedback Control for Vehicle Handling Improvement by Active Steering 125
S. MAMMAR

ELECTRONIC ARCHITECTURE

A Real-Time Platform for Collaboration Projects in Power Train Modeling and Control 131
S. EDLUND, L. ERIKSSON, L. NIELSEN, M. PETTERSSON

Concepts for the Usage of Real-Time Corba in Time-Triggered Architectures 139
O. BARHEINE, K.D. MÜLLER-GLASER

Evaluating Real Time Ability and Failure Propagation in Distributed Systems 147
D. JOHN, U. KIENCKE

Advances of Open-Ended Architecture at the Example of OSEK/VDX 153
R. KRIESTEN, U. KIENCKE

States in Distributed Systems Based Upon Logical Time 161
C. THIERER, P. BORT, U. KIENCKE

Cartronic System Architecture for Energy and Powertrain Management 173
J. LÖFFLER, H. HÜLSER, K. SCHILLER, M. SCHMITT

INTELLIGENT COMPONENTS

Automotive Applications of Rapid Prototyping for Active Vibration Control 181
C. BOHN, H.-J. KARKOSCH, P.M. MARIENFELD, F. SVARICEK

Online Identification of Active Absorbers in Automotive Vibration Control 187
M. BUTTELMANN, B. LOHMANN, P. MARIENFELD, F. SVARICEK, M. VINOGRADSKI, N. NEDELJKOVIC

Digital Voice Enhancement for Improved In-Car Communication 193
K. SCHAAF, J. SCHULTZ, K. TONTCH

Smart Materials and Active Noise and Vibration Control in Vehicles 195
E.J.J. DOPPENBERG, A.P. BERKHOFF, M. van OVERBEEK

Control of Piezoelecric Smart Structures 205
A. KUGI, K. SCHLACHER

Low Temperature Dynamic Characteristics of a Three-Way Catalytic Converter 313
M. BALENOVIĆ, J.M.A. HARMSEN, J.H.B.J. HOEBINK, A.C.P.M. BACKX

H_∞ with Reference Model for Active Suspension System: An *LMI* Approach 319
E. ABDELLAHI, D. MEHDI, R. RAMIREZ MENDOZA, M. M'SAAD

Modelling and Experimental Validation of a Car Starting System 325
F. AMATO, G. CELENTANO, R. IERVOLINO, D. FRENI

Wheel Slip Control by Means of Sluggish Actuators 331
A. ARNOLD, T. BRANDMEIER

ENGINE MODELLING

A Simulation Tool for Predicting Fuel Consumption for Heavy Trucks 339
T. SANDBERG

Modeling of Advanced Control Strategies for Air Flow Sensor 345
G. SAIKALIS, S. OHO, F. LIN

Analysis of an Event-Based Diesel Engine Model for Control Purposes 351
K.J. VANTINE, U. CHRISTEN, K. GLOVER, N. COLLINGS

A New Formulation of Multi-Zone Combustion Engine Models 357
Y. NILSSON, L. ERIKSSON

Isothermal vs. Adiabatic Mean Value SI Engine Models 363
E. HENDRICKS

MODELLING OF COMBUSTION AND TURBO-CHARGING

Modeling of a Turbo Charged SI Engine 369
L. ERIKSSON, L. NIELSEN, J. BRUGÅRD, J. BERGSTRÖM, F. PETTERSSON, P. ANDERSSON

Influence of the Internal Gas Mixture on the Ion Current Signal 379
E. FINKELDEI, M. HART, R. HERWEG, M. KESSLER. G. MÜNKEL, V. WILHELMI

Exhaust Manifold Pressue Estimation on a Turbocharged SI-Engine with Wastegate 385
P. ANDERSSON, L. ERIKSSON

Model Based Exhaust Gas Estimation of a Common Rail Diesel Engine 391
D.D. TORKZADEH, W. LÄNGST, U. KIENCKE

A Hinge Neural Network Approach for the Identification and Optimization of Diesel Engine Emissions 399
C. VLAD, S. TÖPFER, M. HAFNER, R. ISERMANN

Author Index 405

ENGINE CONTROL I

Air-Fuel Ratio Control by Fuzzy Logic, Preliminary Investigation 211
Y. CHAMAILLARD, C. PERRIER

Modelbased Temperature Control for Improved Fuel Economy of SI Engines 217
E. CORTONA, C.H. ONDER, L. GUZZELLA

Fuzzy Modelling, Control and Stability Analysis of an Automotive Engine 223
D. PASSAQUAY, S. BOVERIE, G. HEREDIA, A. OLLERO, A. TITLI, J. ARACIL

Cylinder Air/Fuel Ratio Estimation Using Net Heat Release Data 229
P. TUNESTÅL, J.K. HEDRICK

Control of DISI Engines: Analytical and Experimental Investigations 239
J. SUN, I. KOLMANOVSKY, M. BOESCH, J. DIXON

DIAGNOSTICS

Model Based Diagnosis of the Air Path of an Automotive Diesel Engine 245
M. NYBERG, T. STUTTE, V. WILHELMI

Diagnosis of Evaporative Leaks and Sensor Faults in a Vehicle Fuel System 251
I. ANDERSSON, E. FRISK

Sensor Fault Diagnosis for an Internal Combustion Engine Based on Neural Networks 257
F. MAGNINO, A. FICOLA, M. La CAVA

Fault Detection of a Diesel Injection System by Qualitative Modelling 263
D. FÖRSTNER, J. LUNZE

Vehicle Chassis Monitoring System 271
P. PISU, A. SOLIMAN, G. RIZZONI

ENGINE CONTROL II

Model Based Boost Pressure and Exhaust Gas Recirculation Rate Control for a Diesel Engine with Variable Turbine Geometry 277
J. RÜCKERT, A. SCHLOßER, H. RAKE, B. KINOO, M. KRÜGER, S. PISCHINGER

An Adaptive Estimator of Fuel Film Dynamics in the Intake Port of a Spark Ignition Engine 283
I. ARSIE, C. PIANESE, G. RIZZO, V. CIOFFI

On-Line Design Method of Feedback Controller for Automatic Transmission System 289
R. HIBINO, M. OSAWA, K. KONO, T. SUZUKI

Valve Position Tracking for Soft Landing of Electromechanical Camless Valvetrain 295
W. HOFFMANN, A.G. STEPHANOPOULOU

Robust Nonlinear Torque Control of a Spark Ignition Engine 301
M. SACKMANN, V. KREBS

SUBSYSTEMS

Modeling and Identification of a Leaf Spring System 307
A. CLAVEL, M. SORINE, Q. ZHANG

Copyright © IFAC Advances in Automotive Control,
Karlsruhe, Germany, 2001

DIESEL-ENGINE SPEED CONTROL WITH HANDLING OF DRIVELINE RESONANCES

Magnus Pettersson‡ and Lars Nielsen†

†*Vehicular Systems, Linköping University* ‡*SCANIA AB*
SE-581 83 Linköping *SE-151 87 Södertälje*
E-mail: lars@isy.liu.se,
magnus.pettersson@scania.se

Abstract: A vehicular driveline transfer engine torque to the wheels. Resonances in the elastic parts of the driveline are important to handle when control of the engine and the transmission is optimized. Traditional diesel engine speed control maintains a well damped engine speed set by the driver. However, the resonance modes of the driveline are easily excited by accelerator-position changes or by road disturbances. A speed-control strategy is proposed that includes the behavior of the driveline, and reduces driveline resonances and vehicle shuffle by engine control. Implementation shows significant reduction, also when facing nonlinear torque limitations from maximum torque and diesel smoke delimiters.
Copyright © 2001 IFAC

Keywords: engine control, active damping, power train handling.

1. INTRODUCTION

The main parts of a vehicular driveline are engine, clutch, transmission, shafts, and wheels. Since these parts are elastic, mechanical resonances may occur. The handling of such resonances is basic for functionality and driveability, but is also important for reducing mechanical stress. New driveline-management applications and high-powered engines increase the need for strategies for how to apply engine torque in an optimal way (Kiencke and Nielsen, 2000).

Traditional fuel-injection strategies are of torque control type or speed control type. Control performance is limited by driveline resonances for both control schemes. For diesel engines, speed control is often referred to as RQV (Regler Quer Verstellung) control (Automotive Handbook, 1993). With RQV control there is no active damping of driveline resonances, and for low gears this leads to wheel-speed oscillations known as *vehicle shuffle* (Mo *et al.*, 1996; Pettersson and Nielsen, 1995). The resonance modes are excited by changes in accelerator pedal position or from impulses from towed trailers and road roughness. These oscillations are disturbing to the driver, and more important, limits the response time (from a change in accelerator position to changed wheel speed) of the engine. A desired property with RQV control is a load dependent velocity lag resulting from downhill and uphill driving (Pettersson, 1997).

Low-frequent driveline resonances can be damped by having a strategy that applies engine torque so that the engine inertia is forced to work in the opposite direction of the oscillations. This is referred to as active damping or engine controlled damping of driveline resonances.

In order to derive these strategies, models of the driveline are developed. The aim of the modeling and experiments is to find the most important physical effects that contribute to driveline oscillations. The frequency range of interest includes the first main resonance modes of the driveline. Experiments are performed with a heavy truck with different gears and road slopes in order to excite driveline resonances for modeling.

Model based control is used to extend the RQV control concept with active damping of wheel-speed oscillations, while maintaining the desired velocity lag characteristic for RQV control.

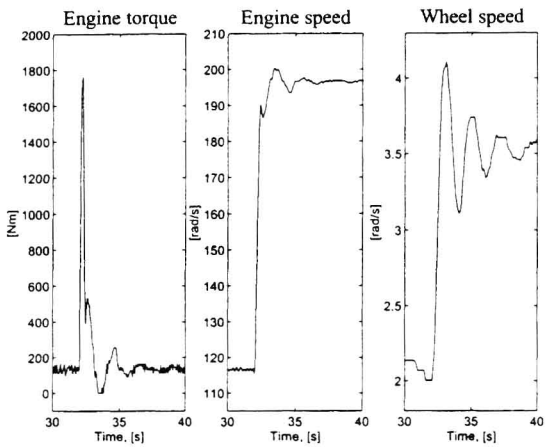

Fig. 1. Measured speed response of a step in accelerator position at t=32 s with a Scania 124L truck. An RQV speed controller is controlling the engine speed with set point 2000 RPM.

2. PROBLEMS WITH DRIVELINE HANDLING

The traditionally used RQV controller is essentially a proportional controller calculating the fuel amount, m_f, as function of the difference between the desired speed set by the driver, r, and the actual measured engine speed, $\dot{\theta}_m$, according to

$$m_f = m_{f0} + K_p(ri - \dot{\theta}_m) \qquad (1)$$

The constant i is the conversion ratio of the driveline, and m_{f0} is a working point dependent constant. The parameter K_p is the controller gain. The reason for this controller structure is the traditionally used mechanical centrifugal governor for diesel pump control (Automotive Handbook, 1993). This means that the controller will maintain the speed demanded by the driver, but with a stationary error (velocity lag), which is a function of the controller gain and the load (rolling resistance, air drag, and road inclination). With a cruise controller, the stationary error is compensated for, which means that the vehicle will maintain the same speed independent of load changes.

A specific example of how the RQV speed controller performs is seen in Fig. 1. The figure shows how the measured engine speed and wheel speed respond to a step input in accelerator position. It is seen how the engine speed is well behaved with no oscillations. With a stiff driveline this would be equivalent with also having well damped wheel speed. However, the more flexible the driveline is, the less sufficient a well damped engine speed is, since the flexibility of the driveline will lead to oscillations in the wheel speed.

If it is desired to decrease the response time of the RQV controller (i.e., increase the bandwidth), the controller gain, K_p in (1), must be increased. Then the amplitude of the oscillations in the wheel speed will be higher.

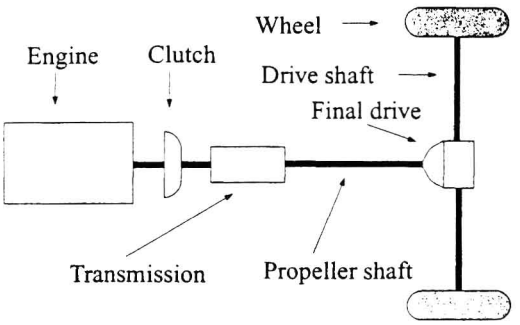

Fig. 2. A vehicular driveline.

2.1 *Goals*

Speed control is the extension of the traditionally used RQV speed control concept with active damping of driveline resonances. The control problems should be formulated so that it is possible to use established techniques and standard automotive sensors to obtain solutions. The designs should be robust against the following limitations:

- The engine torque is not smooth, since the firing pulses result in a pulsating engine torque.
- The output torque of the engine is not exactly known. The only measure is a static torque map from dynamometer tests.
- The engine friction is not known, and must be estimated.
- The engine output torque is limited in different modes of operation. The maximum engine torque is restricted as a function of the engine speed, and the torque level is also restricted at low turbo pressures for smoke prevention.

3. EXPERIMENTAL PLATFORM

Tests were performed with a Scania 124L truck. The driveline of the 6x2 truck (6 wheels, 2 driven) is shown in Fig. 2. The engine is a 12 liter, 6 cylinder turbo-charged DSC12 diesel engine with a unit-pump fuel injection system (Diesel Fuel Injection, 1994). The engine is connected to a manual range-splitter transmission GRS900R via a clutch. The transmission has 14 gears and a hydraulic retarder. The radius of the wheel is $r_w = 0.52$ m, the weight of the truck is $m = 24$ ton, the front area is $A_a = 9\ m^2$, and the drag coefficient is equal to $c_w = 0.6$.

A number of sensors are used along the driveline. The actuator is the diesel engine which is controlled by injecting different amounts of fuel. The truck is equipped with a CAN-bus that connects all control units of the truck. The control algorithms are implemented in a PC with CAN communication (Pettersson, 1997). The engine speed ($\dot{\theta}_m$), the engine temperature

此为试读,需要完整PDF请访问: www.ertongbook.com

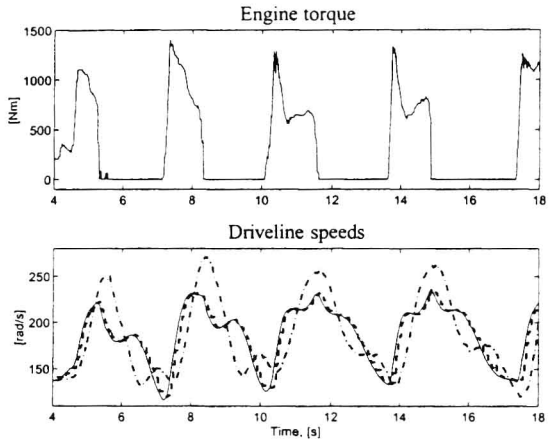

Fig. 3. Logged data on the CAN-bus during step inputs in accelerator position with a Scania 124L truck. Transmission speed (dashed) and wheel speed (dash-dotted) are scaled to engine speed in solid.

(T_m), and the engine torque (M_m) from a static torque map is measured. The transmission speed ($\dot{\theta}_t$) is measured via the transmission node, and the wheel speed ($\dot{\theta}_w$) is measured from the ABS control unit.

3.1 *Experiments*

A number of test roads at Scania were used for testing. They have different known slopes. The variables described above are logged during tests that excite driveline resonances. Fig. 3 shows a test with the 124L truck where step inputs in accelerator position excite driveline oscillations. It is seen that the main flexibility of the driveline is located between the output shaft of the transmission and the wheel (see Fig. 2), since the largest difference in speed is between the measured transmission speed and wheel speed.

4. DRIVELINE MODELING

4.1 *Engine Torque and Friction*

By measuring the amount of fuel, m_f, that is fed to the engine, a measure of the driving torque resulting from the explosions in the cylinders is obtained from dynamometer tests. This torque is labeled $M_m(m_f)$.

The engine friction, M_{fr}, is modeled as a function of the engine speed and the engine temperature (Pettersson, 1997). The resulting friction map is shown in Fig. 4.

4.2 *Control Signal*

The output torque of the engine is the driving torque subtracted by the engine friction. This signal, $u = M_m(m_f) - M_{fr}$, is the torque acting on the driveline, which is a pulsating signal with torque pulses from

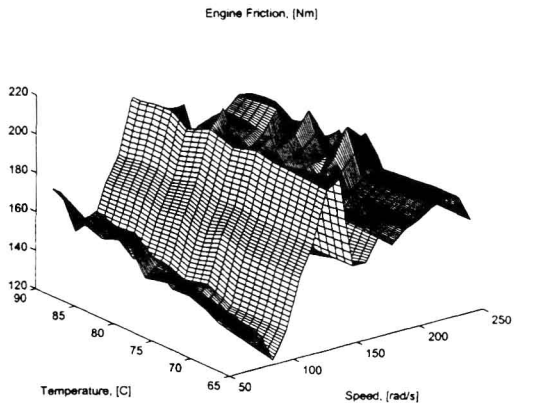

Fig. 4. Engine friction for the 124L truck, modeled as a function of engine speed and engine temperature.

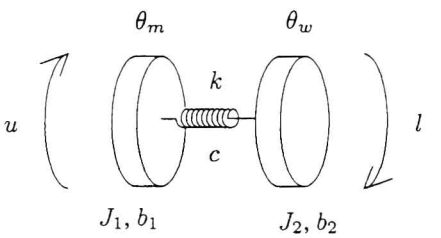

Fig. 5. Driveline model with two inertias connected by a damped torsional drive-shaft flexibility.

each cylinder explosion. However, this control signal, u, is treated as a continuous signal, which is reasonable for the frequency range considered for control design. A motivation for this is that an six-cylinder engine makes 60 strokes/s at an engine speed of 1200 rev/min. This means that a mean-value engine model is assumed (neglects variations during the engine cycle).

4.3 *Main Flexibility*

When studying the driveline during operation, the drive shaft (see Fig. 2) is subject to the relatively largest torsion. This is mainly due to the high torque difference that results from the amplification of the engine torque by the conversion ration of the transmission (i_t) and the final drive (i_f). This number ($i_t i_f$) can be as high as 60 for the lowest gear.

The drive shaft can be modeled as a damped torsional flexibility which leads to the driveline model shown in Fig. 5. The symbols shown in Table 1 are used in the rest of the paper. In Fig. 5, the engine, the clutch, the transmission, and the propeller shaft are lumped together as one rotating inertia, J_1, and the drive shaft connects this inertia to the inertia of the wheel. The wheel inertia is affected by the load, l, which consists of the air drag, rolling resistance, and vehicle mass. Viscous friction is assumed for both the rotating inertias with labels b_1 and b_2. The dynamics of the suspension system is neglected, together with the tires.

J	Mass moment of inertia
i	Conversion ratio
k	Torsional stiffness
c	Torsional damping
b	Viscous friction component
θ	Angle
α	Road inclination
m	Subscript denoting engine
t	Subscript denoting transmission
f	Subscript denoting final drive, fuel
w	Subscript denoting wheel

Table 1. Notations.

By using Newton's generalized second law a mathematical model is formulated (Kiencke and Nielsen, 2000). The state-space representation of this model is

$$\dot{x} = Ax + Bu + H\,l \tag{2}$$

where A, B, H, x, and l are defined as

$$\begin{aligned} x_1 &= \theta_m/i_t i_f - \theta_w \\ x_2 &= \dot{\theta}_m \\ x_3 &= \dot{\theta}_w \\ l &= r_w m\,(c_{r1} + g sin(\alpha)) + \frac{1}{2} c_w A_a \rho_a r_w^3 \dot{\theta}_w^2 \end{aligned} \tag{3}$$

giving

$$A = \begin{pmatrix} 0 & 1/i & -1 \\ -k/iJ_1 & -(b_1 + c/i^2)/J_1 & c/iJ_1 \\ k/J_2 & c/iJ_2 & -(c+b_2)/J_2 \end{pmatrix}, \tag{4}$$

$$B = \begin{pmatrix} 0 \\ 1/J_1 \\ 0 \end{pmatrix}, \quad H = \begin{pmatrix} 0 \\ 0 \\ -1/J_2 \end{pmatrix} \tag{5}$$

where

$$\begin{aligned} i &= i_t i_f \\ J_1 &= J_m + J_t/i_t^2 + J_f/i_t^2 i_f^2 \\ J_2 &= J_w + m r_w^2 \\ b_1 &= b_t/i_t^2 + b_f/i_t^2 i_f^2 \\ b_2 &= b_w + m c_{r2} r_w^2 \end{aligned} \tag{6}$$

with c_{r1} and c_{r2} characterizing the rolling resistance, and ρ the air density. The model is described by three states, and x_2 and x_3 are the engine speed and the wheel speed which can be measured. The first state, x_1, is the drive-shaft torsion, which is not measured.

4.4 *Sensor Location*

A common architectural issue in driveline control is the influence of sensor location. Different sensor locations result in different control problems (Pettersson and Nielsen, 1995). A comparison is made between using feedback from the engine-speed sensor or the wheel-speed sensor. The investigation aims at understanding where to invest in increased sensor performance in future driveline management systems.

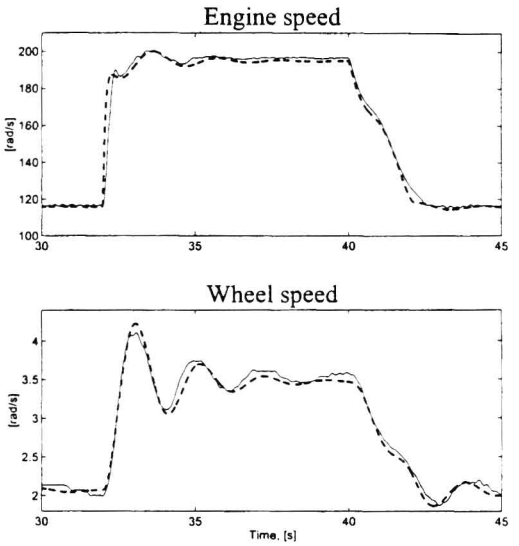

Fig. 6. Measured step response from 1100 RPM to 1900 RPM at t=32 s, with an RQV controller for speed control in solid. Simulations with the same controller and the driveline model is shown in dashed lines. The driveline model captures the main resonance in the measured engine speed and wheel speed.

Two types of disturbances are considered. Load disturbances (v) additive to the load (l), and measurement disturbances (e) additive to the measured output (y), which is specified by the output matrix C. Either the engine speed $\dot{\theta}_m$ ($C = C_m$) or the wheel speed $\dot{\theta}_w$ ($C = C_w$) is used as output giving

$$y = Cx + e \tag{7}$$

with

$$C_m = (0\,1\,0), \quad C_w = (0\,0\,1) \tag{8}$$

The wheel speed, $\dot{\theta}_w$, is the performance output, z, specified by the matrix M as $z = Mx = \dot{\theta}_w$, $M = (0\,0\,1)$. Note that the engine speed sensor can be used ($y = C_m x$) but still the signal that is requested to behave in a certain way is the performance output $z = \dot{\theta}_w$, i.e., the wheel speed.

The measured engine speed and wheel speed are used to estimate the parameters and initial conditions of the driveline model. The data is separated in two sets used for estimation and validation respectively. The prediction error estimation method (PEM) (Ljung, 1995) is used for estimation, with the material data of the unknowns as initial parameter guess. Fig. 6 shows validation of model structure and parameters in a closed-loop test. Field trials are performed with the 124L truck with an RQV fuel-injection controller controlling the engine speed from 1100 RPM to 1900 RPM at $t = 32$ s. The same controller is used in simulations with the driveline model (2)-(6) with parameters estimated for the 124L truck. There is good agreement between model outputs and experiments, which shows that the model captures the main resonance in the engine speed and the wheel speed.

5. COST FUNCTION

The speed control problem can be described as minimizing the difference between the actual speed and the reference value, $(\dot{\theta}_w - r)$, but with a control signal, u, possible to realize by the diesel engine. This can be formulated in a cost criterion, consisting of two terms. The first term is $(\dot{\theta}_w - r)^2$, which describes the deviation in speed. The second term describes the deviation in control signal from the level needed to obtain $\dot{\theta}_w = r$. Let this level be u_0, which will be derived later. The criterion is described by

$$\lim_{T\to\infty} \int_0^T (\dot{\theta}_w - r)^2 + \eta(u - u_0)^2 \qquad (9)$$

The controller that minimizes this cost function is called the *speed controller*. Active damping of driveline resonances will be obtained since $(\dot{\theta}_w - r)^2$ is minimized. The trade-off between rise time and control signal amplitude is controlled by tuning the parameter η.

The control signal, u, can take negative values, since if the fuel injection is turned off, the control signal is equal to the engine friction which is negative. This level is about 200 Nm according to Fig. 4. The maximum value of the control signal is restricted by the delimiters described in Section 2, which means that between 1000 and 1800 Nm is possible to generate, depending on driving situation.

The constant u_0 is derived by solving the driveline equations for a stationary point. For a given wheel speed, $\dot{\theta}_w$, and load, l, the driveline has the following stationary point

$$\begin{aligned} x_0(\dot{\theta}_w, l) &= \begin{pmatrix} b_2/k & 1/k \\ i & 0 \\ 1 & 0 \end{pmatrix} \begin{pmatrix} \dot{\theta}_w \\ l \end{pmatrix} \\ &= \delta_x \dot{\theta}_w + \delta_l l \end{aligned} \qquad (10)$$

$$\begin{aligned} u_0(\dot{\theta}_w, l) &= \begin{pmatrix} (b_1 i^2 + b_2)/i & 1/i \end{pmatrix} \begin{pmatrix} \dot{\theta}_w \\ l \end{pmatrix} \\ &= \lambda_x \dot{\theta}_w + \lambda_l l \end{aligned} \qquad (11)$$

This means that the torque u_0 is a function of the reference value, r, and the load, l.

The controller that minimizes (9) has no stationary error in the wheel speed, since the load l is included and thus compensated for. A stationary error comparable with that of the RQV controller can be achieved by using only a part of the load, l, as will be demonstrated in Section 6.1.

6. SPEED CONTROLLER DERIVATION

The problem formulation (9) will be treated in two steps. First, without a stationary error characteristic for RQV control, and then extending the strategy to include this type of stationary error. The cost function (9) is in this section solved with LQG technique (Maciejowski, 1989). This is done by linearizing the driveline model and rewriting (9) in terms of the linearized variables. A state-feedback matrix is derived that minimizes (9).

The model (2) is affine since it includes a constant term l. The model is linearized in the neighborhood of a stationary point (x_0, u_0). The linear model is

$$\Delta\dot{x} = A\Delta x + B\Delta u \qquad (12)$$

where Δ expresses deviations from the stationary point given by (10) and (11). Note that the linear model is the same for all stationary points.

The cost function is expressed in Δx and Δu as

$$\lim_{T\to\infty} \int_0^T (M\Delta x + r_1)^2 + \eta(\Delta u + r_2)^2 \qquad (13)$$

with

$$\begin{aligned} r_1 &= Mx_0 - r \\ r_2 &= u_0 - u_0(r, l) \end{aligned} \qquad (14)$$

The constants r_1 and r_2 are expressed as state variables by augmenting the plant model (A, B) with models of the constants r_1 and r_2. The augmented state variable is $x_r = (\Delta x^T \; r_1 \; r_2)^T$, which the gives the new state matrices A_r and B_r (Pettersson, 1997). By using these equations, the cost function (13) is written in the form

$$\lim_{T\to\infty} \int_0^T x_r^T Q x_r + R\Delta u^2 + 2x_r^T N \Delta u \qquad (15)$$

with

$$\begin{aligned} Q &= (M\ 1\ 0)^T (M\ 1\ 0) + \eta(0\ 0\ 0\ 0\ 1)^T (0\ 0\ 0\ 0\ 1) \\ N &= \eta(0\ 0\ 0\ 0\ 1)^T \\ R &= \eta \end{aligned} \qquad (16)$$

The cost function (13) is minimized by using

$$\Delta u = -K_c x_r \qquad (17)$$

with

$$K_c = Q^{-1}(B_r^T P_c + N^T) \qquad (18)$$

where P_c is the solution to the Riccati equation

$$A_r^T P_c + P_c A_r + R - (P_c B_r + N) Q^{-1} (P_c B_r + N)^T = 0 \qquad (19)$$

The control law (17) becomes

$$u = K_0 x_{30} + K_l l + K_r r - \begin{pmatrix} K_{c1} & K_{c2} & K_{c3} \end{pmatrix} x \qquad (20)$$

with

$$\begin{aligned} K_0 &= \begin{pmatrix} K_{c1} & K_{c2} & K_{c3} \end{pmatrix} \delta_x - K_{c4} M \delta_x + \lambda_x - K_{c5} \lambda_x \\ K_r &= K_{c4} + K_{c5} \lambda_x \\ K_l &= \begin{pmatrix} K_{c1} & K_{c2} & K_{c3} \end{pmatrix} \delta_l - K_{c4} M \delta_l + \lambda_l \end{aligned} \qquad (21)$$

where δ_x, δ_l, λ_x, and λ_l are described in (10) and (11).

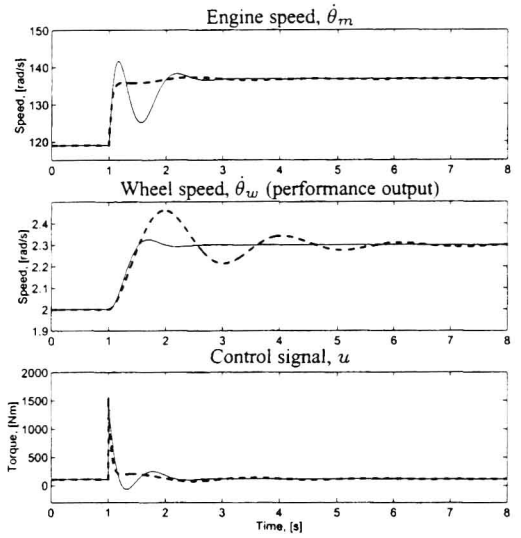

Fig. 7. Response of step in accelerator position at t=1 s. The driveline model is controlled with the speed control law (20) in solid lines. RQV control (1) is seen in dashed lines.

A step-response simulation with the speed controller (20) is shown in Fig. 7, with gear 1, $l = 3000$ Nm, $\eta = 5 \cdot 10^{-8}$, and $\alpha = 0.0001$. The peak value of the control signal is about the same for the two controllers. However the overshoot is significantly reduced when using the speed controller (20) compared to the RQV controller (1). The driving torque is controlled such that the oscillations in the wheel speed are actively damped. This means that the controller applies the engine torque in a way so that the engine inertia works in the opposite direction of the oscillation. Then the engine speed oscillates, but the important wheel speed is well behaved as seen in Fig. 7.

6.1 *Extending with RQV Behavior*

The RQV controller has no information about the load, l, and therefore a stationary error will be present when the load is different from zero. The speed controller (20) is a function of the load, and the stationary error is zero if the load is estimated and compensated for. There is however a demand from the driver that the load should give a stationary error, and it should be zero only when using a cruise controller.

The speed controller can be modified such that a load different from zero gives a stationary error. This is done by using βl instead of the complete load in (20). The constant β ranges from $\beta = 0$ which means no compensation for the load, to $\beta = 1$ which means fully compensation of the load and no stationary error. The compensated speed control law becomes

$$u = K_0 x_{30} + K_l \beta l + K_r r - \begin{pmatrix} K_{c1} & K_{c2} & K_{c3} \end{pmatrix} x \quad (22)$$

In Figure 8, the RQV controller with its stationary error (remember the reference value $r = 2.3$ rad/s) is compared to the compensated speed controller (22) for

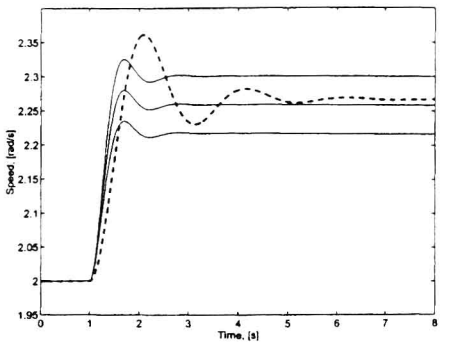

Fig. 8. Wheel-speed response of step in accelerator position at t=1 s. The driveline model is controlled with the RQV controller (1) in dashed line, and the speed controller with stationary error (22) with $\beta = 0,\ 0.5,\ 1$ in solid lines.

three values of β. By adjusting β, the speed controller with active damping is extended with a stationary error comparable with that of the RQV controller.

7. INFLUENCE FROM SENSOR LOCATION

The speed controller (20) uses feedback from all states ($x_1 = \theta_m/i_t i_f - \theta_w$, $x_2 = \dot{\theta}_m$, and $x_3 = \dot{\theta}_w$). A sensor measuring shaft torsion (e.g., x_1) is normally not used, and therefore an observer is needed to estimate the unknown states. In this work, either the engine speed or the wheel speed is used as input to the observer. This results in different control problems depending on sensor location. Especially the difference in disturbance rejection is investigated.

The observer gain is calculated using Loop-Transfer Recovery (LTR) (Maciejowski, 1989). Two different observer problems result depending on which sensor location is used. The speed controller (20) becomes

$$u = K_0 x_{30} + K_r r + K_l l - \begin{pmatrix} K_{c1} & K_{c2} & K_{c3} \end{pmatrix} \hat{x} \quad (23)$$

with K_0, K_r, and K_l given by (21). The estimated states $\hat{x}$ are given by the Kalman filter

$$\Delta\dot{\hat{x}} = A\Delta\hat{x} + B\Delta u + K_f(\Delta y - C\Delta\hat{x}) \quad (24)$$

$$K_f = P_f C^T V^{-1} \quad (25)$$

where P_f is found by solving the Riccati equation

$$P_f A^T + A P_f - P_f C^T V^{-1} C P_f + W = 0 \quad (26)$$

The covariance matrices W and V corresponds to disturbances v and e respectively. The output matrix C is either equal to C_m or C_w in (8).

To recover the properties achieved in the previous design step when all states are measured, the following values are selected

$$V = 1, \quad W = \rho B B^T \quad (27)$$

$$C = C_m \ or \ C_w, \quad \rho = \rho_m \ or \ \rho_w$$

and solving (25) and (26) for K_f.

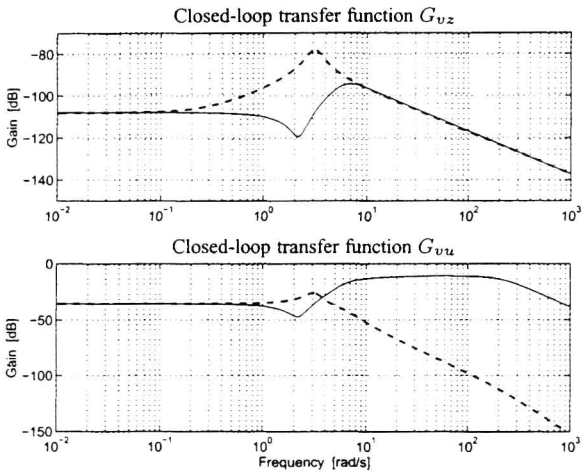

Fig. 9. Closed-loop transfer functions from load disturbance v to performance output z and control signal u. Feedback from $\dot{\theta}_w$ is shown in solid and feedback from $\dot{\theta}_m$ is shown in dashed lines. With $\dot{\theta}_m$ feedback the transfer functions have a resonance peak, resulting from the open-loop zeros.

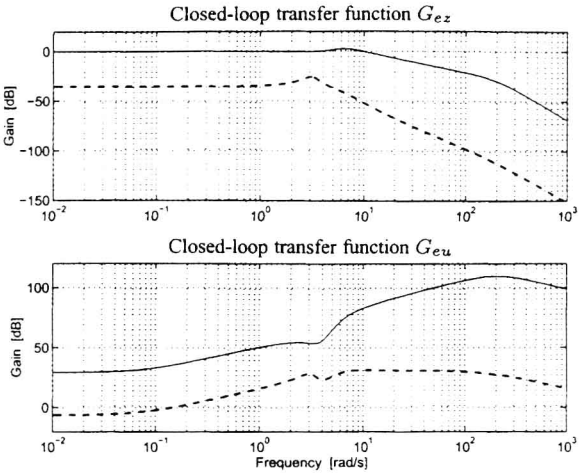

Fig. 10. Closed-loop transfer functions from measurement noise e to performance output z and control signal u. Feedback from $\dot{\theta}_w$ is shown in solid and feedback from $\dot{\theta}_m$ is shown in dashed. Measurement disturbances are better attenuated with engine speed feedback.

When using LQG with feedback from all states, the phase margin, φ, is at least 60° and the amplitude margin, a, is infinity as stated before. This is obtained also when using the observer by increasing ρ towards infinity. For the simulation case presented in Fig. 7, the following values are used

$$\rho_m = 5 \cdot 10^5 \;\Rightarrow\; \varphi_m = 60.5°,\;\; a_m = \infty \quad (28)$$

$$\rho_w = 10^{14} \;\Rightarrow\; \varphi_w = 59.9°,\;\; a_w = 35.0 \quad (29)$$

where the aim has been to have at least 60° phase margin.

The observer dynamics is cancelled in the transfer function from reference value to performance output ($z = \dot{\theta}_w$) and control signal (u). Hence, these transfer functions are not affected by sensor location. However, the observer dynamics will be included in the transfer functions from disturbances v and e to both z and u.

Influence from Load Disturbances Fig. 9 shows how the performance output and the control signal are affected by the load disturbance v. There is a resonance peak in G_{vz} (transfer function from signal v to signal z) when using feedback from the engine speed sensor, which is not present when feedback from the wheel speed sensor is used. The reason for this can be seen when studying the closed-loop transfer function G_{vz}

$$(G_{vz})_{cl} = \frac{G_{vw}}{1 + G_{uw}F_y} \quad (30)$$

when the sensor measures the wheel speed, and

$$(G_{vz})_{cl} = \frac{G_{vw} + F_y(G_{um}G_{vw} - G_{uw}G_{vm})}{1 + G_{um}F_y} \quad (31)$$

when the sensor measures the engine speed (Pettersson, 1997). The subscript cl stands for closed loop, and F_y is the controller. Hence, when using the wheel speed sensor, the controller is not present in the numerator, and when the engine speed sensor is used, the controller is present.

The optimal return ratio in the LQG step is (Maciejowski, 1989)

$$K_c(sI - A)^{-1}B \quad (32)$$

Hence, in the optimal return ratio, the poles from A is kept, but there are new zeros that are placed such that the relative degree of (32) is one, the phase margin is at least 60°, and the gain margin is infinite. In the LTR step the return ratio is

$$F_y G_{uy} = K_c(sI - A - BK_c - K_f C)^{-1}K_f C(sI - A)^{-1}B \quad (33)$$

When ρ in (27) is increased towards infinity, (32) equals (33). This means that the zeros in the open-loop system $C(sI - A)^{-1}B$ are cancelled by the controller. Hence, the open-loop zeros will become poles in the controller F_y. This means that the closed-loop system will have the open-loop zeros as poles when using the engine speed sensor. Thus, G_{vz} will have the poles $-0.52 \pm 3.08i$ causing the resonance peak in Fig. 9.

Influence from Measurement Disturbances The influence from measurement disturbances e is seen in Fig. 10. The closed-loop transfer function G_{ez} can be rewritten as

$$(G_{ez})_{cl} = -\frac{G_{uz}F_y}{1 + G_{uy}F_y} \quad (34)$$

When ρ in (27) is increased towards infinity, (32) equals (33). Then (34) gives

$$(G_{ez})_{cl,m} = (G_{ez})_{cl,w}\,\frac{G_{uw}}{G_{um}} \quad (35)$$

where cl, m and cl, w means closed loop with feedback from $\dot{\theta}_m$ and $\dot{\theta}_w$ respectively.

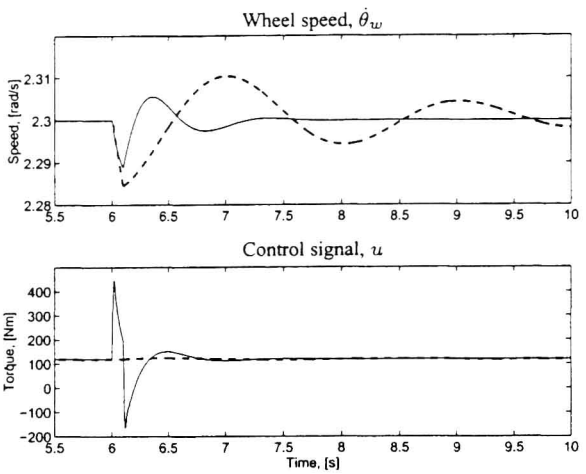

Fig. 11. Simulated load impulse disturbance at t=6 s. The solid line corresponds to $\dot{\theta}_w$-feedback and feedback from $\dot{\theta}_m$ is seen in dashed line. The load impulse generates a control signal that damps the impulse disturbance when feedback from the wheel-speed sensor is used, but not with engine-speed feedback.

Hence, the difference in G_{ez} depending on sensor location is described by the dynamic output ratio $G_{w/m} = G_{uw}/G_{um}$ (Pettersson and Nielsen, 1995). Measurement disturbances are better attenuated with engine speed feedback. The difference in low-frequency level is equal to the conversion ratio of the driveline as can be seen in Fig. 10. Therefore, this effect increases with lower gears.

8. EVALUATION

8.1 *Influence from disturbances*

An important step in a principle simulation study is that such disturbances can be introduced that hardly can be generated in systematic ways in real experiments. One such example is impulse disturbances from a towed trailer. Disturbance rejection is demonstrated by simulating a more complete nonlinear driveline model (Pettersson, 1997), briefly described in Section 4, with the speed controller (23) and the observer (24) based on the reduced driveline model with drive-shaft flexibility.

The simulation case presented here is a load impulse disturbance simulated at t=6 s at an engine speed of about 1300 RPM with gear 1. The disturbance is generated as a square pulse with 0.1 s width and 1200 Nm height, and both feedback principles are simulated. Fig. 11 shows the result of the simulation.

The load impulse disturbance is better attenuated with feedback from the wheel-speed sensor, which is a verification of the behavior that was discussed in Section 7.

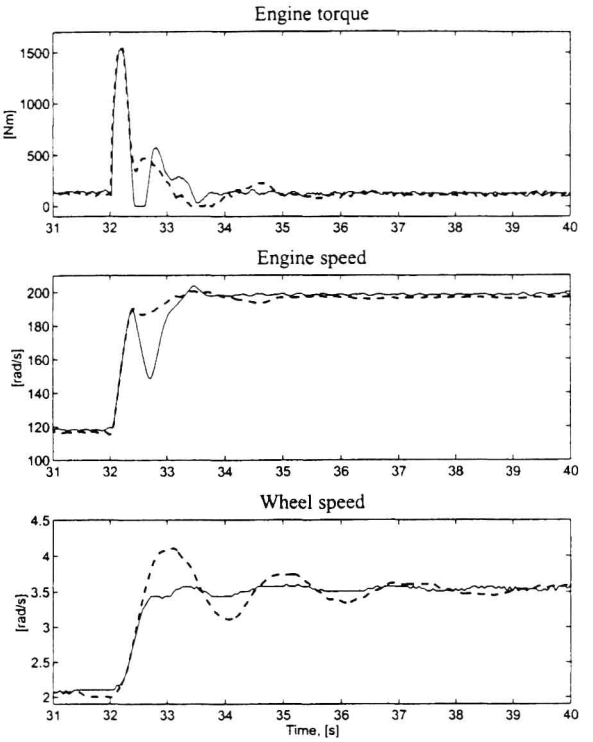

Fig. 12. Speed step at t=32 s with active damping and engine-speed feedback (solid) compared to traditional RQV control with K_p=50 (dashed). Experiments are performed without smoke delimiter on a flat road. After 32.5 s, the control signals differ depending on control scheme. With speed control, the engine inertia works in the opposite direction of the oscillations, which are significantly reduced.

8.2 *Field Trials*

Field trials are performed with the 124L truck on an almost flat test road with a minimum of changes from test to test. The focus of the tests is low gears, with low speeds and thus little impact from air drag. The speed controller (23) and the observer (24) are discretized by Tustin's method (Franklin *et al.*, 1990), and implemented with a sampling time of 50 Hz.

The test presented here is a velocity step response from 2.1 rad/s to 3.6 rad/s (about 1200 RPM to 2000 RPM) with gear 1. At first the smoke delimiter (see Section 2) is not used in order to be able to investigate the control design with as small restrictions on the control signal as possible.

In Fig. 12, the speed controller is compared to traditional RQV control. The engine torque, the engine speed, and the wheel speed are shown. The speed controller uses feedback from the engine speed, and the RQV controller has the gain $K_p = 50$. With this gain the rise-time and the peak torque output is about the same for the two controllers. A high torque output is possible because no smoke delimiter is used.

此为试读,需要完整PDF请访问: www.ertongbook.com